Hindawi
Advances in Civil Engineering
Volume 2023, Article ID 2227326, 13 pages
https://doi.org/10.1155/2023/2227326

*Research Article*

# Forward Modeling and Model Test of Ground-Penetrating Radar toward Typical Asphalt Pavement Distresses

**Zhijun Liu**,[1] **Tao Sun**,[2] **Tao Huang**,[1] **Guoqiang Liu**,[1] **Yunhan Tao**,[1] **Gaoxin Wang**,[1] **and Liangliang Wang**[1]

[1]*School of Mechanics and Civil Engineering, China University of Mining and Technology, Xuzhou 221116, China*
[2]*Shanghai Municipal Engineering Design Institute (Group) Co., Ltd, Shanghai 200000, China*

Correspondence should be addressed to Zhijun Liu; liuzhijun0331@163.com

Received 22 July 2023; Accepted 18 August 2023; Published 11 September 2023

Academic Editor: Timo Saksala



As the total mileage of roads with asphalt concrete pavement is increasing rapidly, using ground-penetrating radar (GPR) to estimate the dimension of internal distresses of the asphalt pavement is of great significance for pavement maintenance. However, the relationship between the dimension of road distress and the characteristics of road distress's radar echo has not been quantified. Therefore, in this paper, a GPR forward modeling toward base cracks and interlayer voids is conducted to investigate the relationship, and a model test is conducted to verify the forward modeling. The results indicate that it is feasible to use a GPR image to estimate the dimension of interlayer voids and base cracks. For vertical dimension estimation, the vertical dimension of the distressed area has a positive relationship with the difference in the return time of radar echoes from the top and bottom of the distressed area. However, the area's vertical dimension must be at least a quarter of the length of the electromagnetic wave used in the GPR to be correctly identified. Otherwise, it is not easy to distinguish the overlapping echoes from each other. For horizontal dimension estimation, the base crack's horizontal dimension has a quadratic correlation with the echo's amplitude, and the horizontal dimension of an interlayer void is approximately equal to the length of its echo's flat segment.

## 1. Introduction

It is well known that crack is a common distress of asphalt pavement, mainly divided into fatigue crack and base crack. Base cracks usually develop from bottom to top in the pavement structure, so they are not easy to detect or estimate in the early time of development [1–3]. Once the base crack invades the surface course, the water seeping into the road surface will gather in the crack and destroy the connection between the base and the surface, leading to layer debonding and forming a void between the two layers [4]. Even if the position of distresses has been obtained by ground-penetrating radar (GPR), both base cracks and interlayer voids are challenging to be treated at a proper time that considers both economy and safety. Therefore, a method of estimating the dimension of subsurface distresses is in demand.

Some scholars have investigated the feasibility of nondestructive detection of the road distresses using GPR. Solla et al. [5, 6] verified the applicability of GPR and infrared thermal imaging in detecting cracks in the asphalt pavement and believe that these two techniques can estimate the depth of cracks, detect the presence of filler material, and initially identify the source and dimension of the cracks. Krysinski and Sudyka [7] carried out long-term monitoring of three roads in operation by GPR and summarized the features of cracks in GPR images. Torbaghan et al. [8] proposed a method to detect cracks automatically using GPR and determined that the minimum size of detectable cracks is about 1.1–1.3 mm.

The research mentioned above is based on the prototype or model tests, which are limited by the diversity of pavement distresses and the control of experimental variables. For this reason, GPR forward modeling, a kind of numerical analysis unlimited in the experimental conditions, is used for forming a comprehensive theory to explain the complex and variable phenomena in practical engineering.

The forward modeling of GPR toward asphalt pavement distress was investigated in the several areas, such as vertical

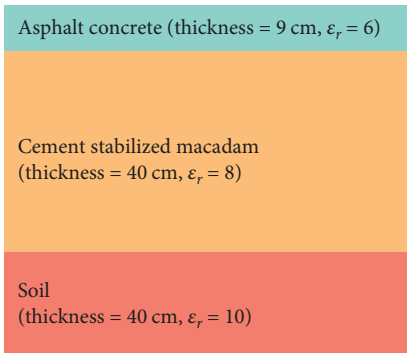


Figure 1: The diagram of the basic model.

Table 1: Parameters of GPR forward modelling.

| Parameters | Value |
|---|---|
| Model size (m) | $1 \times 0.6$ |
| Space grid step size (m) | $0.002 \times 0.002$ |
| Time window (ns) | 20 |
| Initial transmitting antenna coordinate (m) | (0.02, 0.58) |
| Initial receiving antenna coordinate (m) | (0.17, 0.58) |
| Antenna step length (m) | 0.01 |
| Incentive source type | Ricker |
| Excitation source frequency (MHz) | 900 |

crack identification, water-filled or air-filled void identification, and distinguishing between reflection cracks and fatigue cracks [9–13]. These researches fully demonstrate the feasibility of using forward modeling results to guide the analysis and interpretation of GPR data [14, 15].

In this paper, using GprMax, a GPR forward modeling toward base cracks and interlayer voids was conducted to investigate the relationship between the dimension of the two distresses and the features of their radar images for providing a theoretical and technical basis for the quantitative estimation of the dimension of typical asphalt pavement distresses by GPR. Moreover, a model test was conducted to verify the result of forward modeling.

## 2. Basic Model of Forward Modeling

The principal parameters of the model are the number, dimensions, and electrical properties of the pavement structure layers.

In this paper, the basic model structure refers to the typical second-class highway pavement structure in Jiangsu, China [16]. Considering that the material inside the surface course is similar, the entire surface course is assumed to be the same homogeneous medium. Same for the base course and subgrade. The sittings of the model layers are as follows: the surface course is 9 cm thick asphalt concrete with a relative permittivity of 6; the base course is 40 cm thick cement stabilized macadam with a relative permittivity of 8; the subgrade is soil with a relative permittivity of 10 [17]. The schematic diagram of the model is shown in Figure 1.

Pavement materials are generally dry, so they can be regarded as an ideal medium whose conductivity is close to zero. The materials are also nonferromagnetic, so their relative permeability is close to one [18]. The value of related parameters of the model is shown in Table 1. Besides, the model is based on the following assumptions: the materials of the medium in the model are isotropic; the electrical properties of the materials are invariant under the changes in frequency; the $Z$ direction is a continuous extension in space without boundaries.

As the material of each layer is assumed to be homogeneous and the reflection of the electromagnetic wave will only happen where the permittivity changes, the echo should appear at the border of each layer. The result of forward modeling toward the basic model is shown in Figure 2. Two reflected waves appear at 3 and 11 ns, respectively. That is the same as expected and proves that using GprMax to simulate the process of scanning pavement structures with GPR is feasible.

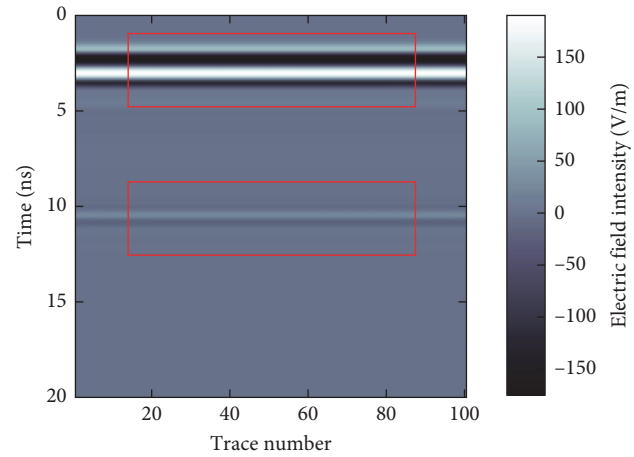


Figure 2: The result of GPR forward modeling toward the basic model.

## 3. Forward Modeling toward a Base Crack

*3.1. Features of Base Cracks in GPR Image.* In order to obtain the features of base cracks in the GPR image, add base cracks to the basic model. Figure 3 shows a model consisting of the basic model and a 20 cm high and 1 cm wide crack. Figure 4 shows the result of forward modeling toward the model. It can be noticed that the echo of the crack in the GPR image is a clear hyperbola with a small amplitude (compared with the echo of the junction of the surface course and base course). Besides, there are a few noises near the echo due to the diffraction of electromagnetic waves.

*3.2. Influence of the Crack's Horizontal Dimension on Its Radar Echo.* A series of models with a single crack of different horizontal dimensions is created to investigate the influence of the changes of the crack's horizontal dimension on its radar echo. As the horizontal dimension of a base crack is generally between 0.1 and 2 cm [19, 20], the horizontal

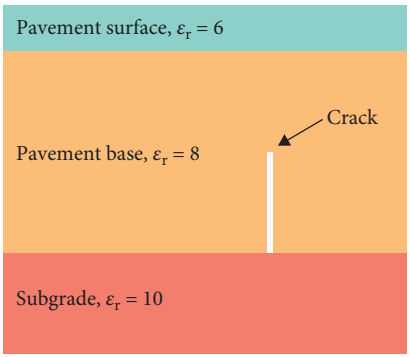


Figure 3: The diagram of the model with a base crack.

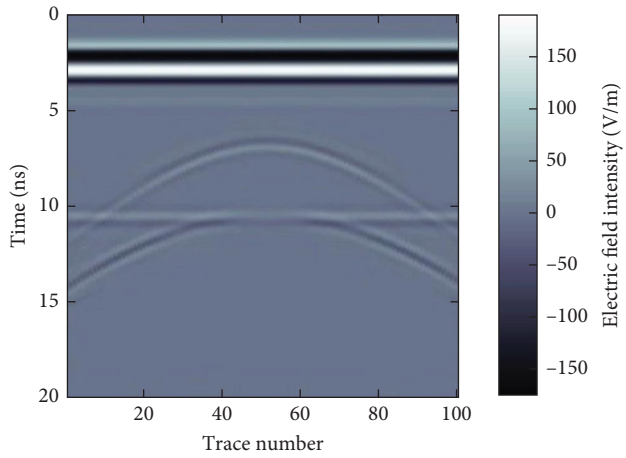


Figure 4: The result of GPR forward modeling toward the model with a crack.

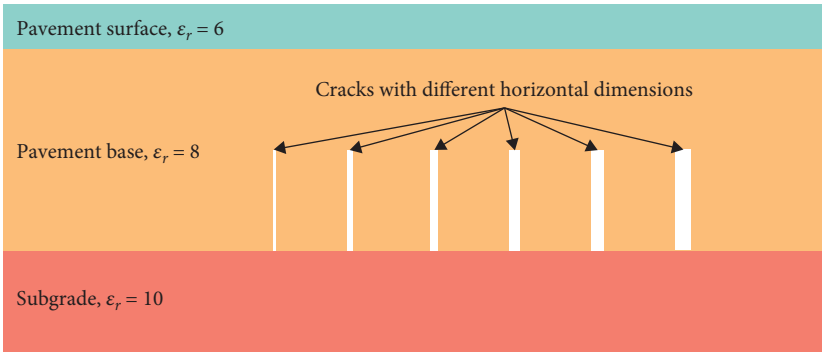


Figure 5: Models with a crack of different horizontal dimensions.

dimension of cracks in those models is set to 0.5, 1, 1.5, 2, 2.5, and 3 cm, respectively.

Figure 5 shows the series of models with a single crack of different horizontal dimensions (combined into one image for comparison), and Figure 6 shows the results of forward modeling toward these models.

The shape of the crack's echo is almost invariant under the change of horizontal dimension. However, the echo amplitude has a pretty clear relationship with the crack's horizontal dimension. More specifically, the larger the crack's horizontal dimension, the larger the echo amplitude. The result of fitting the echo amplitude and the crack's horizontal dimension is shown in Figure 7 and Equation (1).

$$A = 2.715w^2 + 4.397w + 3.532 (R^2 = 0.997), \quad (1)$$

where $A$ is the maximum value of the echo amplitude, which is normalized, of the crack's top surface and $w$ is the horizontal dimension of the crack.

Obviously, there is a clear quantitative relationship between the crack's horizontal dimension and the echo

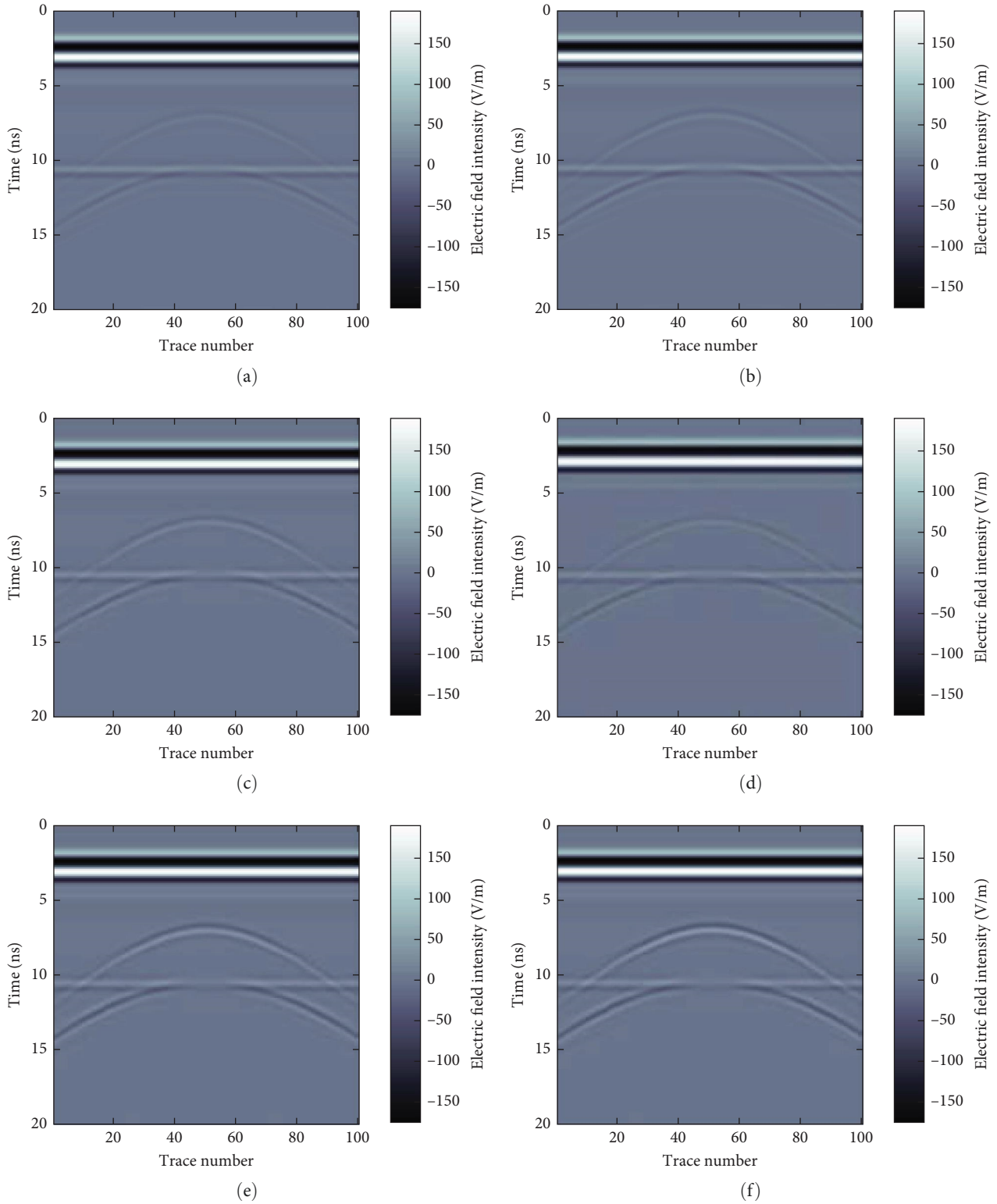


Figure 6: Results of forward modelling toward models with a crack of different horizontal dimensions (a–f).

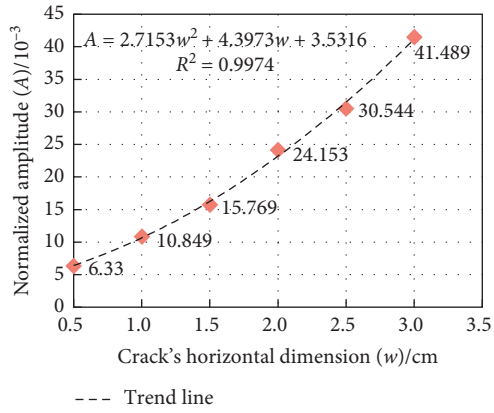


Figure 7: The relationship between $A$ and $w$.

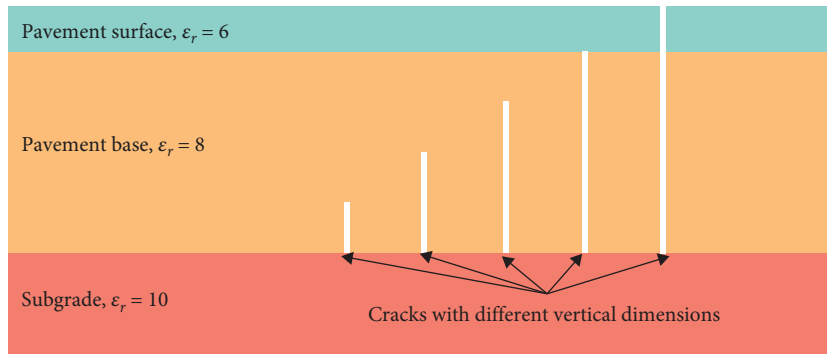


Figure 8: Models with a crack of different vertical dimensions.

amplitude based on Equation (1). However, the coefficients in Equation (1) are not constant. It will be affected by changes in the relative permittivity of the detection object [21]. In other words, the relationship shown in Equation (1) should be redetermined once the road material changes.

*3.3. Influence of the Crack's Vertical Dimension on Its Radar Echo.* A series of models with a single crack of different vertical dimensions is created to investigate the influence of the changes of the crack's vertical dimension on its radar echo. The vertical dimension of the crack in those models is set at 10, 20, 30, 40, and 49 cm, respectively. Figure 8 shows the series of models with a crack of different vertical dimensions, and Figure 9 shows the results of forward modeling toward these models.

According to the results shown in Figure 9, the time distance of the two echoes belonging to the top and bottom surfaces of the crack is positively correlated with the crack's vertical dimension. The relationship between the time distance and the crack's vertical dimension is shown in Figure 10.

The quantitative relationship between the time distance and the crack's vertical dimension can be derived as follows:

If the base crack is inside the base course,

$$T = \sqrt{\frac{\varepsilon_{rb}[4(h+d)^2 + b^2]}{c^2}} - \sqrt{\frac{\varepsilon_{rb}[4(h+d-L)^2 + b^2]}{c^2}}. \quad (2)$$

If the base crack has invaded the surface course (across the whole pavement),

$$T = \sqrt{\frac{\varepsilon_{rb}(4h^2 + b^2)}{c^2}} + \sqrt{\frac{\varepsilon_{rs}(4d^2 + b^2)}{c^2}} - \sqrt{\frac{\varepsilon_{rs}[4(h+d-L)^2 + b^2]}{c^2}}, \quad (3)$$

where $T$ is the time distance of two echoes belonging to the top and bottom surfaces of the crack; $L$ is the crack's vertical dimension; $\varepsilon_{rb}$ and $\varepsilon_{rs}$ are the relative permittivity of base course and surface course, respectively; $h$ and $d$ are the thickness of the surface course and base course, respectively; $b$ is the distance between transmit and receive antennas; $c$ is the speed of light which is 0.3 m/ns constantly.

Equations (2) and (3) can be used for estimating the vertical dimension of base cracks after obtaining the time distance by GPR in the actual project.

## 4. Forward Modeling toward an Interlayer Void

*4.1. Features of Interlayer Voids in GPR Image.* A model consists of the basic model, a crack through the whole pavement, and a void derived from the crack is shown in Figure 11. The void is 20 cm wide, 2 cm height, and filled with air.

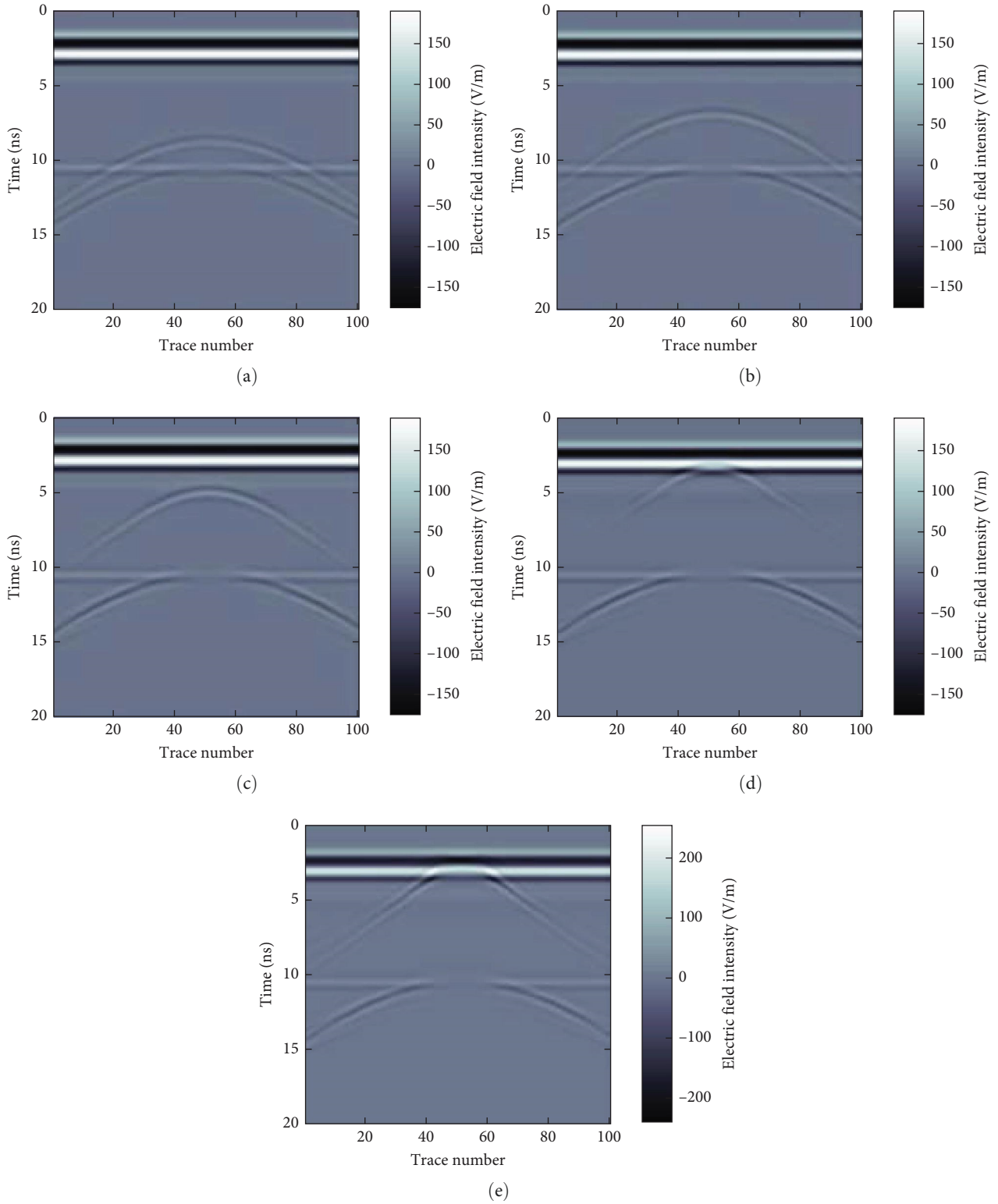


Figure 9: Results of forward modeling toward models with a crack of different vertical dimensions (a–e).

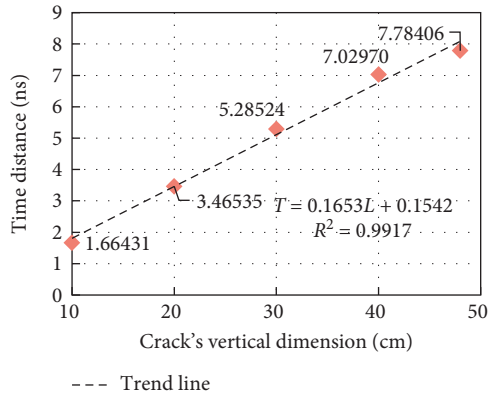


Figure 10: The relationship between the time distance and the crack's vertical dimension.

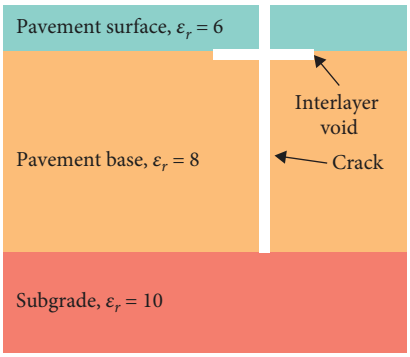


Figure 11: The diagram of the model with an interlayer void.

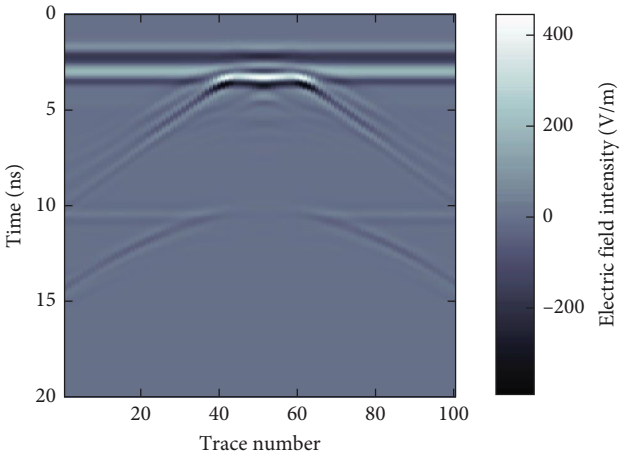


Figure 12: The result of GPR forward modeling toward the model with an interlayer void.

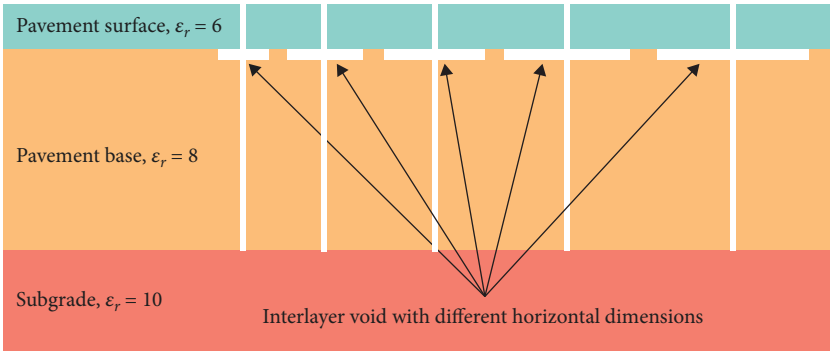


Figure 13: Models with a void of different horizontal dimensions.

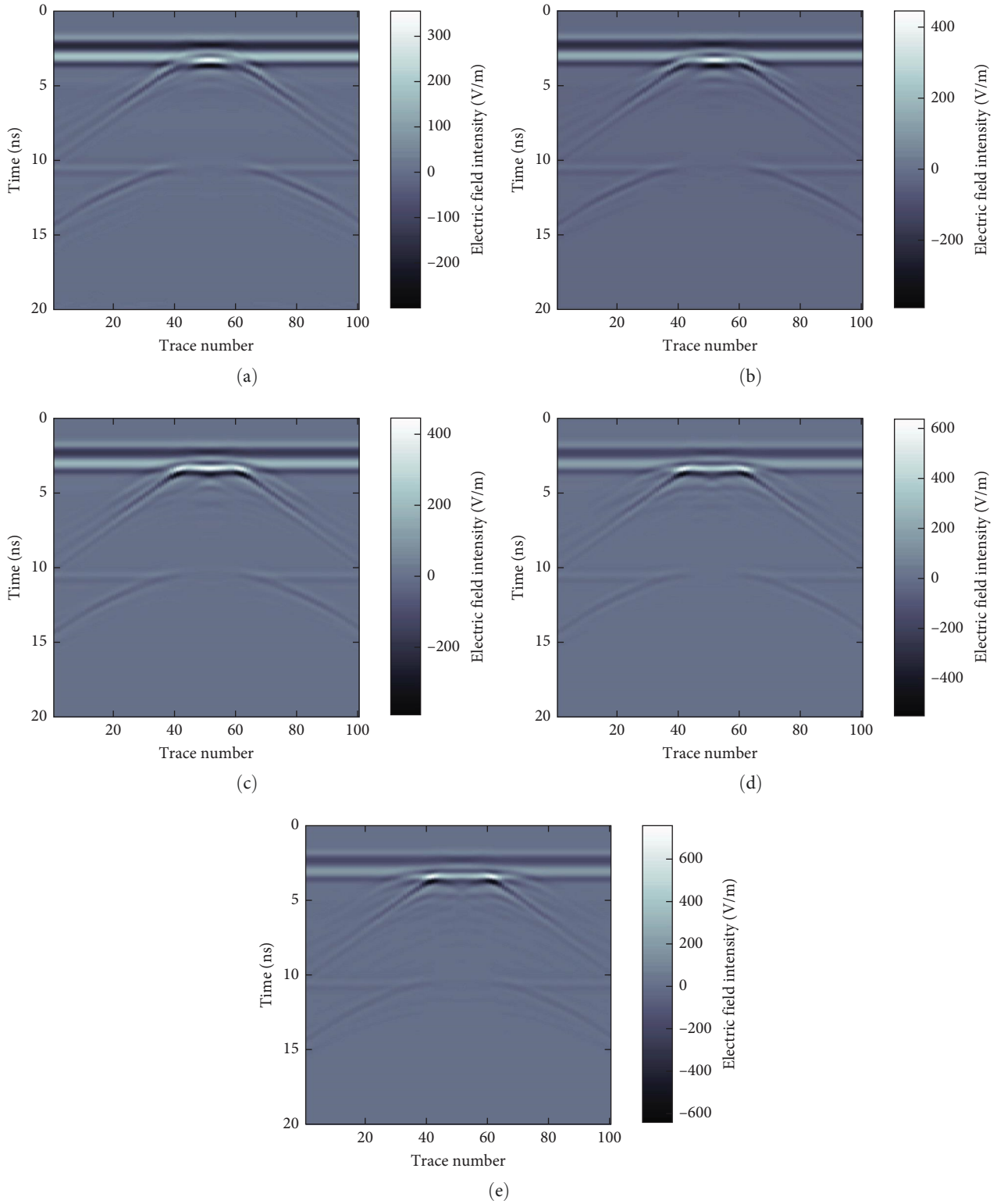


Figure 14: Results of forward modeling toward models with a void of different horizontal dimensions (a–e).

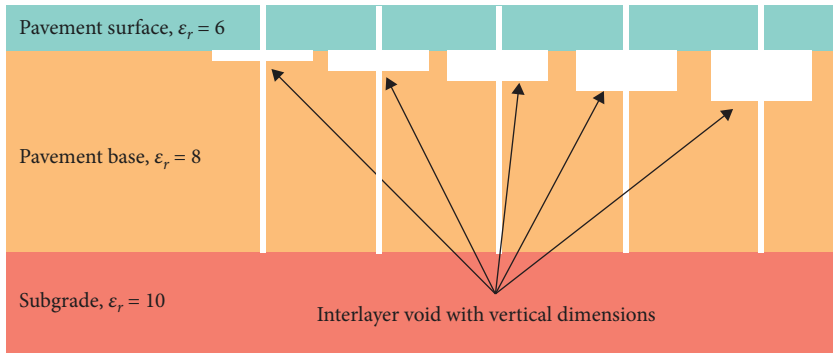


Figure 15: Models with a void of different vertical dimensions.

Figure 12 shows the result of forward modeling toward the model.

The GPR echo of an interlayer void consists of a flat wave in the middle and some noises on the sides. The flat wave comes from the reflection of the interlayer void, and the noises come from the diffraction of the void edge.

*4.2. Influence of the Void's Horizontal Dimension on Its Radar Echo.* A series of models with a void of different horizontal dimensions, which is set at 10, 15, 20, 25, and 30 cm, respectively, is created to investigate the influence of the changes of the void's horizontal dimension on its radar echo. The range of the void's horizontal dimension depends on the phenomenon that the interlayer void generally does not excessively exceed the area where the tire touches the ground [22], which is about 20 cm long and 20 cm wide. Figure 13 shows the models, and Figure 14 shows the results of forward modeling toward these models.

It can be noticed that there is a clear positive correlation between the length of the echo's flat segment and the void's horizontal dimension. Considering that the trace number is generally replaced by the coordinates of the sampling points in the actual project, the length of the flat segment is approximately equal to the horizontal dimension of the void. This conclusion can be used for estimating the horizontal dimension of an interlayer void.

*4.3. Influence of the Void's Vertical Dimension on Its Radar Echo.* A series of models with a void of different vertical dimensions, which is set at 2, 4, 6, 8, and 10 cm, respectively, is created to investigate the influence of the changes of the void's vertical dimension on its radar echo. Figure 15 shows these models, and Figure 16 shows the results of forward modeling toward these models.

Limited by the vertical resolution of GPR, the echoes belonging to the top and bottom surfaces of the void will overlap if the void's vertical dimension is too small. More specifically, the two echoes will be challenging to distinguish from each other if the void's vertical dimension is less than a quarter of the wavelength of the electromagnetic wave used in GPR [23].

## 5. Model Test for GPR Forward Modeling

In order to verify the results of GPR forward modeling toward the two pavement distresses, a series of models containing distresses of different dimensions are built.

*5.1. Model Design.* For GPR, the difference between different materials is essentially the difference in permittivity, which mainly affects the amplitude and speed of the electromagnetic wave. In other words, the shape of the echo is mainly related to the distress's spatial structure, not the type of material. Besides, this paper mainly aims to estimate the dimension of road distresses. Therefore, the asphalt pavement, cement stabilized macadam, and distress area are replaced by a marble slab, sandy soil, and solid acrylic plate, respectively, in the models to carry out the test more conveniently.

Figure 17 shows the structure of the model. A box, which is 1.2 m long, 0.5 m wide, 0.5 m height, and made of acrylic board, is used as a container for models. Fill the box with 40 cm thick sandy soil, and put a 9 cm thick marble slab on the sandy soil. Use SIR-4000 with 900 MHz antenna to scan the model.

*5.2. Result of Model Test.* Build a series of models according to the structures shown in Figures 5, 8, and 13, and scan those models by GPR. Through the analysis of the data, the following conclusions are drawn:

(i) There has a good quadratic relationship between the crack's horizontal dimension and the echo amplitude. Therefore, the method of estimating a crack's horizontal dimension with its echo amplitude is reliable. Figure 18 and Equation (4) show the relationship between the crack's horizontal dimension and the normalized echo amplitude determined by the model test.

$$A = 3.2357w^2 - 0.9593w + 40.21 (R^2 = 0.896), \quad (4)$$

where the definitions of $A$ and $w$ have been described in Equation (1).

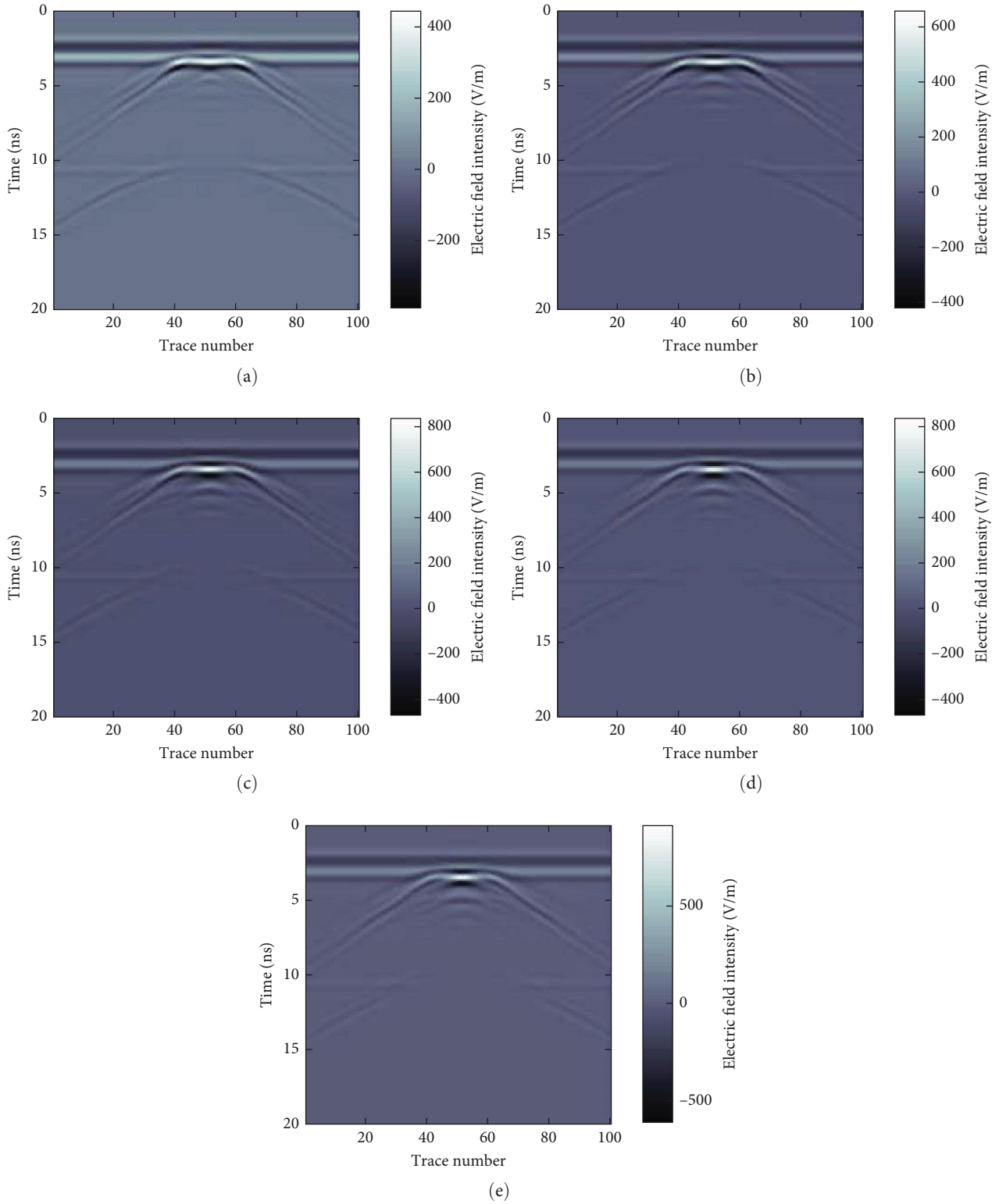


Figure 16: Results of forward modeling toward models with a void of different vertical dimensions (a–e).

(ii) The time distance increases linearly with increasing vertical dimension in the model test. Furthermore, the time distance from the model test is lower than that from the theoretical calculation under a same vertical dimension. However, the relative error of the time distance obtained by the two methods is less than 12%, and it decreases with the increase of the crack's vertical dimension. Figure 19 shows the relationship among the crack's vertical dimension, the time distance of echoes determined by the

(a) (b) (c)

Figure 17: The model and its scanning scene: (a) A solid acrylic plate to simulate the disease area; (b) appearance of the entire model; and (c) GPR scanning scene.

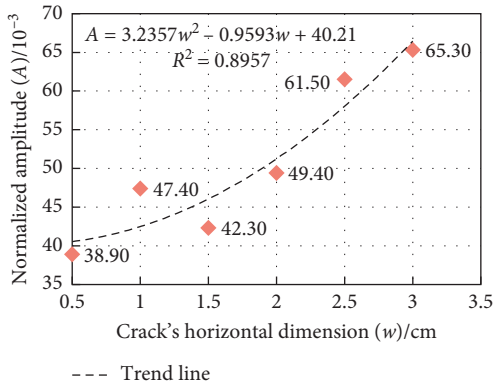


Figure 18: The relationship between the echo's normalized amplitude and the crack's horizontal dimension.

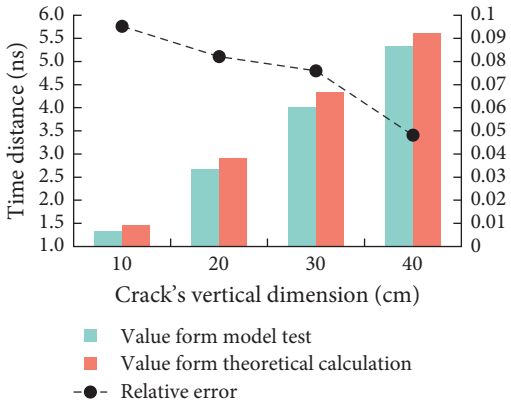


Figure 19: The relationship between the crack's vertical dimension and the time distance of echoes.

Table 2: The length of echo's flat segment obtained by GPR.

| Void's horizontal dimension (cm) | 10 | 15 | 20 | 25 | 30 |
|---|---|---|---|---|---|
| The length of the echo's flat segment (cm) | 10.15 | 15.25 | 20.36 | 25.51 | 30.55 |
| Relative error (%) | 1.50 | 1.67 | 1.80 | 2.04 | 1.83 |

model test, and the time distance determined by Equation (2).

(iii) The length of the echo's flat segment shown in Table 2 is approximately equal to the void's horizontal dimension, with a maximum error of 2.04% and an average error of 1.77%, which is consistent with the rule obtained from the forward modeling.

## 6. Conclusions

(i) The echo of the base crack is a clear hyperbola, and the echo of an interlayer void consists of a flat wave in the middle and some noises on the sides.

(ii) A quadratic relationship exists between the horizontal dimension of the base crack and the echo amplitude. A linear relationship exists between the vertical dimension of the base crack and the time distance of the two echoes from the top and bottom surfaces of the crack. Those two rules can be used for estimating the dimension of base cracks.

(iii) The horizontal dimension of an interlayer void is approximately equal to the flat segment length of the echo of its top surface. This rule can be used for estimating the dimension of an interlayer void. However, it needs the void's vertical dimension to be more than a quarter of the wavelength of the electromagnetic wave used in GPR.

(iv) The same rules are obtained from forward modeling and model test, which means that the echo features of base cracks and interlayer voids obtained by forward modeling are reliable.

(v) The actual structure of pavement distress is far more complex than the model in this paper. In further research, the structure of the model should be further refined according to the actual distress to improve the reliability and practicability of the forward modeling results.

## Data Availability

All data used to support the findings of this study are available from the corresponding author upon request.

## Conflicts of Interest

The authors declare that there is no conflict of interest regarding the publication of this paper.

## Acknowledgments

This work was supported by the National Natural Science Foundation of China under grant number 51908545. We thank the China University of Mining and Technology and Xuzhou Shirun Traffic Engineering Testing Co., Ltd. for providing instruments and laboratories.

## References

[1] Y. Xin, D. Yinfei, A. K. Ariffin, S. Abdullah, A. Ali, and A. Muchtar, "Numerical simulation of reflective crack forming in semi-rigid asphalt pavement subjected to traffic load," in *Fracture and Strength of Solids Vii, Pts 1 and 2*, M. J. Ghazali and Z. Sajuri, Eds., vol. 1 and 2, pp. 599–604, Trans Tech Publications Ltd., Stafa-Zurich, 2011.

[2] D. Zhang, Q. Li, Y. Chen, M. Cao, L. He, and B. Zhang, "An efficient and reliable coarse-to-fine approach for asphalt pavement crack detection," *Image and Vision Computing*, vol. 57, pp. 130–146, 2017.

[3] L. Huang, P. Zhang, Z. Hu, and W. Wu, "Research on thermal crack fatigue propagation of asphalt pavement with semi-rigid base," *Highway Engineering*, vol. 45, no. 5, pp. 79–83, 2020.

[4] Y. Miao, Y. Wan, and Y. Dong, "Numerical simulation of thermal stress for reflective crack of asphalt pavement," *Rock and Soil Mechanics*, vol. 28, no. S1, pp. 343–347, 2007.

[5] M. Solla, H. González-Jorge, M. Varela, and H. Lorenzo, "Ground-penetrating radar for inspection of in-road structures and data interpretation by numerical modeling," *Journal of Construction Engineering and Management*, vol. 139, no. 6, pp. 749–753, 2013.

[6] M. Solla, S. Lagüela, H. González-Jorge, and P. Arias, "Approach to identify cracking in asphalt pavement using GPR and infrared thermographic methods: preliminary findings," *NDT&E International*, vol. 62, pp. 55–65, 2014.

[7] L. Krysiński and J. Sudyka, "GPR abilities in investigation of the pavement transversal cracks," *Journal of Applied Geophysics*, vol. 97, pp. 27–36, 2013.

[8] M. E. Torbaghan, W. Li, N. Metje, M. Burrow, D. N. Chapman, and C. D. F. Rogers, "Automated detection of cracks in roads using ground penetrating radar," *Journal of Applied Geophysics*, vol. 179, Article ID 104118, 2020.

[9] L. Cheng-Mi, Q. Zhen, Z. Hai-Long, and L. Xiu-Zhong, "Practical methods for detection of concealed cracks in highway pavement using ground penetration radar data," *The Chinese Journal of Geophysics*, vol. 50, no. 5, pp. 1558–1568, 2007.

[10] Y. Bao, R. Gao, D. Guo, S. Bai, and X. Xin, "Forward modelling and detection of GPR in Urban road base disease," in *Iaeds15: International Conference in Applied Engineering and Management*, P. Ren, Y. Li, and H. Song, Eds., Aidic Servizi Srl, Milano, 2015.

[11] T. X. H. Luo, W. W. L. Lai, and A. Giannopoulos, "Forward modelling on GPR responses of subsurface air voids," *Tunnelling and Underground Space Technology*, vol. 103, Article ID 103521, 2020.

[12] X. Yan, "Model test of road disease ground penetrating radar and forward simulation of GprMax," *Modeling and Simulation*, vol. 10, no. 1, pp. 114–120, 2021.

[13] S. Guo, Z. Xu, X. Li, and P. Zhu, "Detection and characterization of cracks in highway pavement with the amplitude variation of GPR diffracted waves: insights from forward modeling and field data," *Remote Sensing*, vol. 14, no. 4, Article ID 976, 2022.

[14] J. Sudyka, L. Krysinski, A. Zofka, T. Mechowski, and P. Harasim, "Identification of deep-rooted transverse cracks using ground penetrating radar," in *Resilient and Safe Road Infrastructure*, vol. 356 of *IOP Conference Series: Materials Science and Engineering*, IOP Publishing Ltd, Kielce, Poland, Article ID 012022, May 2018.

[15] L. Gao, Y. Luo, H. Song, G. Kong, and G. Hu, "Forward simulation signal of underground pipeline based on ground

penetrating radar," *Russian Journal of Nondestructive Testing*, vol. 56, no. 11, pp. 936–947, 2020.

[16] Z. Liu, X. Wei, D. Wang, and L. Wang, "Performance of cement-stabilized macadam roads based on aggregate gradation interpolation tests," *Mathematical Biosciences and Engineering*, vol. 16, no. 4, pp. 2371–2390, 2019.

[17] M. Yang, H. Fang, F. Wang, Y. Wang, X. Du, and J. Lei, "First-order symplectic Euler method for ground penetrating radar forward simulations in dispersive medium," *Construction and Building Materials*, vol. 299, Article ID 123904, 2021.

[18] N. Diamanti and D. Redman, "Field observations and numerical models of GPR response from vertical pavement cracks," *Journal of Applied Geophysics*, vol. 81, pp. 106–116, 2012.

[19] Z. Yao, J. Lian, and X. Ren, "Mechanical responses of base cracking in semi-rigid pavement," *Rock and Soil Mechanics*, no. 12, pp. 2250–2254, 2006.

[20] Y. Wang, F. Ni, and X. Ma, "Stress comparison of asphalt pavements with different base crack states," *Journal of Traffic and Transportation Engineering*, vol. 8, no. 6, pp. 34–39, 2008.

[21] F. M. Fernandes and J. C. Pais, "Virtual special issue ground-penetrating radar and complementary non-destructive testing techniques in Civil Engineering Laboratory observation of cracks in road pavements with GPR," *Construction and Building Materials*, vol. 154, pp. 1130–1138, 2017.

[22] C. Song and J. Ning, "Influence of complete local void in middle and lower surface layers on the stress of three-layer asphalt pavement surface," *Journal of Chongqing Jiaotong University (Natural Science)*, vol. 36, no. 12, pp. 43–46, 2017.

[23] U. S. Khan, "Near real time automatic interpretation of ground penetrating radar data for utility detection," *Ph.D*, 2010, November 2022, https://www.proquest.com/docview/1788102783/abstract/8F50EB5D60924211PQ/1.